PERGAMON

International Journal of Heat and Mass Transfer 44 (2001) 4323–4331

International Journal of HEAT and MASS TRANSFER

www.elsevier.com/locate/ijhmt

Critical heat flux prediction for saturated flow boiling of water in vertical tubes

Gian Piero Celata [a,*], Kaichiro Mishima [b], Giuseppe Zummo [a]

[a] *ENEA, Energy Department, Institute of Thermal Fluid Dynamics, Via Anguillarese 301, 00060 S.M. Galeria, Rome, Italy*
[b] *Research Reactor Institute, Kyoto University, Kumatori-cho, Sennan-gun, Osaka 590-04, Japan*

Received 31 August 2000; received in revised form 5 January 2001

Abstract

This study presents a new analytical model for the prediction of the critical heat flux (CHF) in water saturated flow boiling in round vertical and uniformly heated pipes. The CHF is assumed to occur in annular flow when the liquid film vanishes at the exit section of the heated channel. Channel pressure drop is calculated using the Friedel correlation. Liquid film flow rate is obtained by a balance of liquid entrainment and droplet deposition. Two mechanisms are considered in the calculation of the entrainment: liquid–vapour interfacial waves and boiling in the liquid film. The model CHF prediction values are compared with a data set of 5159 selected experimental points for water, showing a good agreement both in precision and in accuracy for liquid quality in the range 0.2–1.0.

Keywords: Boiling; Modeling; Two-phase flow

1. Introduction

The critical heat flux (CHF) is an important design limitation for many industrial boiling systems and is crucial for safety operations of water cooled nuclear reactors. A remarkable feature of the CHF in saturated flow boiling is that in many applications, it occurs in annular flow regime. Annular flow is a particularly important flow regime, since it occurs along the major part of the vapour quality range (roughly from around 0.1 up to unity), for a wide range of pressure and flow conditions. Under this regime a liquid film covers the surface of the heated tube, and while vapour with entrained droplets flows in the central core. The CHF occurs when the liquid film on the heater dries out. Therefore, the CHF in this region is referred to as dryout. Several models such as the Whalley et al. [1], Saito et al. [2] and Sugawara [3] have been developed to calculate the CHF using empirical correlations for droplet entrainment and deposition. These models are successful in predicting the CHF for many practical conditions. It turned out, however, that they overpredicted the CHF for short tubes. The present model, based on the model of Mishima et al. [4], which has been initially developed for water at atmospheric pressure, is extended over a wide range of tube geometry and inlet conditions.

2. Analytical model

2.1. Reference conditions

The two-phase flow reference conditions at the CHF in the heated channel are represented in Fig. 1. The channel is assumed to be uniformly heated. There are three main heat transfer regions: single phase flow region, subcooled flow boiling region and saturated flow boiling region. Generally, in the saturated flow boiling region, the flow pattern varies from bubbly, to slug, to churn and finally eventually to annular flow. The annular flow regime is characterised by the presence of a liquid film flowing on the heated wall, a vapour core stream in the centre of the channel, and entrained

* Corresponding author. Tel.: +39-06-3048-3905; fax: +39-06-3048-3026.
E-mail address: celata@casaccia.enea.it (G.P. Celata).

0017-9310/01/$ - see front matter
PII: S0017-9310(01)00072-2

Nomenclature

A	area (m^2)
c_p	specific heat at constant pressure (J kg^{-1} K^{-1})
d	droplet deposition rate (kg m^{-2} s^{-1})
D	tube diameter (m)
D_b	vapour bubble diameter (m)
e	droplet entrainment rate (kg m^{-2} s^{-1})
E	fraction of liquid flowing as droplets in the vapour core
e_w	wave droplet entrainment rate (kg m^{-2} s^{-1})
e_B	boiling droplet entrainment rate (kg m^{-2} s^{-1})
E_∞	equilibrium entrainment fraction
f	friction factor
$f(\beta)$	function of contact angle β introduced by Staub [10]
Fr	Froude number $G^2/(gD\rho^2)$
G	mass flux (kg m^{-2} s^{-1})
g	gravitational acceleration (m s^{-2})
h	heat transfer coefficient (W m^{-2} K^{-1})
i	enthalpy (J kg^{-1})
k	thermal conductivity (W m^{-1} K^{-1})
j	volumetric flux or superficial velocity (m s^{-1})
$N_{\mu l}$	viscosity number
p	pressure (MPa)
q''	heat flux (W m^{-2})
Re	Reynolds number GD/μ
T	temperature (°C)
u	velocity (m s^{-1})
u^+	non-dimensional velocity
y^+	non-dimensional distance
w	liquid mass flow rate (kg s^{-1})
We	Weber number $G^2D/(\rho\sigma)$
x	steam quality
Z	channel length (m)

Greek symbols

α	void fraction
β	liquid contact angle
δ	liquid sublayer thickness (m)
ΔT_{sat}	$T_{wall} - T_{sat}$ (K)
ε	surface roughness (m)
λ	latent heat of vaporisation (J kg^{-1})
μ	dynamic viscosity (kg s^{-1} m^{-1})
η	non-dimensional parameter used in the Ishii Mishima correlation
ρ	density (kg m^{-3})
ρ_{TP}	homogeneous density (kg m^{-3})
σ	surface tension (N m^{-1})
τ	shear stress (N m^{-2})
Φ_{lo}	Friedel two-phase multiplier

Subscripts

ex	pertains to the exit conditions
exp	experimental value
Fri	parameters of the Friedel correlation
in	pertains to the inlet conditions
l	pertains to the liquid phase
le	pertains to the entrained liquid phase
lf	pertains to the liquid film
m	mean value
ONB	onset of nucleate boiling
sat	pertains to the saturated conditions
SP	pertains to the single phase conditions
sub	pertains to the subcooled conditions
v	pertains to the vapour phase

droplets in the vapour core. The liquid film flow rate decreases along the heated channel due to the liquid evaporation and droplet entrainment. Under these conditions, and for uniformly heated conditions of the channel, CHF occurs when the liquid film flow rate is reduced to zero and the heated wall dries out at the channel outlet.

The pressure drop of in the heated channel is evaluated by taking into account of pressure losses in each region represented in Fig. 1. For each region the most appropriate pressure drop calculation method has been chosen.

2.2. Flow regions boundaries

In order to perform the pressure drop calculations in each flow region (Fig. 1), it is important to define the boundaries and the extensions of the different regions. In Fig. 1, the extension of single phase flow, subcooled flow boiling and saturated flow boiling regions are indicated,

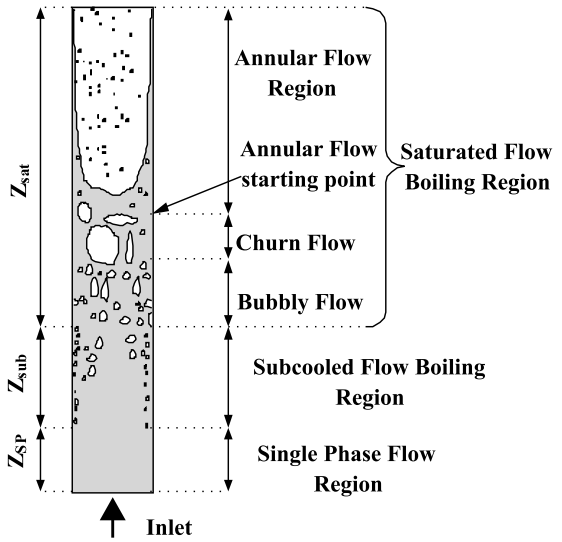

Fig. 1. Two-phase flow patterns in the heated channel.

respectively, with Z_{SP}, Z_{sub} and Z_{sat}. For the calculation of Z_{SP}, Z_{sub} and Z_{sat}, the following well-known equations are used in the model.

The boundary between the single phase and the subcooled flow boiling regions is located in the point, where wall temperature (T_{wall}) exceeds the value typical for the onset of nucleate boiling:

$$T_{wall} \geqslant T_{sat} + |\Delta T_{sat}|_{ONB}, \tag{1}$$

being T_{sat} the liquid saturation temperature and

$$|\Delta T_{sat}|_{ONB} = T_{ONB} - T_{sat} \tag{2}$$

is the superheat necessary for nucleation incipience. Wall temperature can be calculated with

$$T_{wall}(z) = T_{in} + \frac{q''}{h} + \frac{4q''z}{Gc_{pl}D}, \tag{3}$$

where h is the single phase heat transfer coefficient given by the well-known Dittus–Boelter [5] correlation. The wall superheat at the onset of nucleate boiling, $|\Delta T_{sat}|_{ONB}$, is calculated with the Bergles and Rohsenow correlation [6]:

$$|\Delta T_{sat}|_{ONB} = 0.555\left(\frac{q''}{1082p^{1.156-1}}\right)^{p^{0.0234}/2.16} \tag{4}$$

where p (bar), ΔT_{sat} (K), q'' (W m^{-2}). Re-arranging Eqs. (3) and (4) it is possible to obtain the following expression for the single phase length Z_{SP}:

$$Z_{sp} = \left((T_{sat} + |\Delta T_{sat}|_{ONB}) - (T_{in} + q''/h)\right)\frac{Gc_{pl}D}{4q''}. \tag{5}$$

In the subcooled flow boiling region, the local liquid quality is

$$x(z) = \frac{4q''}{D\lambda G} + \frac{i_{l,sat} - i_{l,in}}{\lambda},$$

where $i_{l,sat}$ and $i_{l,in}$ are the local saturation enthalpy and the inlet liquid enthalpy, respectively.

The boundary between the saturated and the subcooled regions is the location along the channel where the quality is zero. Therefore the length of the subcooled flow boiling region is given by the following expression:

$$Z_{sub} = |Z|_{x=0} - Z_{SP}. \tag{6}$$

Knowing the extensions of single phase and subcooled flow boiling regions, the length of the saturated flow boiling region is calculated with

$$Z_{sat} = Z - Z_{sub} - Z_{SP}. \tag{7}$$

2.3. Pressure drop calculation

The total pressure drop in the heated channel is calculated using the following equation:

$$\Delta p = \Delta p_{SP} + \Delta p_{sub} + \Delta p_{sat}. \tag{8}$$

Each term in the above equation refers to the different regions represented in Fig. 1. In the single phase region the pressure drop is evaluated using integrating from 0 up to Z_{SP} (see Fig. 1) along the channel, the following equation

$$\frac{dp_{SP}}{dz} = f_0\frac{G^2}{2D\rho_l} + \rho_l g. \tag{9}$$

The friction factor f_0 is $f_0 = f(\mu_{wall}/\mu_l)^{0.25}$. This correction is proposed by Kays and Crawford [7] accounting for the temperature effect on the liquid viscosity. The friction factor f_0 is that obtained using the Blasius equation $f = 0.3164Re^{-0.25}$, while μ_{wall} is the liquid viscosity evaluated at wall temperature while, and μ_b is the liquid viscosity at the bulk temperature. The term $\rho_l g$, is the static head pressure.

In the subcooled flow boiling region, the pressure drop is calculated as integrating the following expression from Z_{SP} up to Z_{sub}:

$$\frac{dp_{sub}}{dz} = f\frac{G^2}{2D\rho_l} + \rho_l g. \tag{10}$$

In this equation the friction factor f is evaluated using the Colebrook–White [8] equation combined with the Levy's [9] rough surface model for subcooled flow boiling, i.e.:

$$\frac{1}{\sqrt{f}} = 1.14 - 2\log_{10}\left(\frac{\varepsilon}{D} + \frac{9.35}{Re\sqrt{f}}\right), \tag{11}$$

where the surface roughness ε, as suggested by Levy, is assumed to be as $\varepsilon = 0.75D_b$, and where D_b is the departure vapour bubble diameter calculated using the Staub model [10]:

$$D_b = \frac{32}{f}\frac{\sigma f(\beta)\rho_l}{G^2}. \tag{12}$$

Here, σ is the surface tension, and $f(\beta)$ is a function of the liquid contact angle β; for water Staub suggested $f(\beta) = 0.02$ to 0.03. In the present model $f(\beta) = 0.03$ is used.

In the saturated flow boiling region pressure drop Δp_{sat} is calculated using the Friedel [11] correlation. According to Lezzi and Niro [12], who compared different pressure drop correlations with experimental pressure loss measurements under CHF conditions in water saturated flow boiling, the Friedel correlation provided the best performance.

In the saturated flow boiling region the pressure drop Δp_{sat} is calculated by integrating from Z_{sub} up to Z the following equation:

$$\frac{\mathrm{d}p_{\mathrm{sat}}}{\mathrm{d}z} = f_{\mathrm{l}}\frac{G^2}{2D\rho_{\mathrm{l}}}\Phi_{\mathrm{lo}}^2 + G^2 + \frac{\mathrm{d}}{\mathrm{d}z}\left(\frac{x^2}{\alpha\rho_{\mathrm{v}}} + \frac{(1-x)^2}{(1-\alpha)\rho_{\mathrm{l}}}\right) + g(\alpha\rho_{\mathrm{v}} + (1-\alpha)\rho_{\mathrm{l}}) \tag{13}$$

being the first term $f_{\mathrm{l}}(G^2/2D\rho_{\mathrm{l}})\Phi_{\mathrm{lo}}^2$, the frictional pressure drop. In Eq. (13), f_{l} is the friction factor calculated as the mass flow is completely liquid and Φ_{lo} is the Friedel two phase multiplier:

$$\Phi_{\mathrm{lo}}^2 = E_{\mathrm{Fri}} + \frac{3.24F_{\mathrm{Fri}}H_{\mathrm{Fri}}}{Fr^{0.045}We^{0.035}}, \tag{14}$$

$$E_{\mathrm{Fri}} = (1-x)^2 + x^2\left(\frac{\rho_{\mathrm{l}}f_{\mathrm{v}}}{\rho_{\mathrm{v}}f_{\mathrm{l}}}\right)$$
$$F_{\mathrm{Fri}} = x^{0.78}(1-x)^{0.24}, \tag{15}$$

$$H_{\mathrm{Fri}} = \left(\frac{\rho_{\mathrm{l}}}{\rho_{\mathrm{v}}}\right)^{0.91}\left(\frac{\mu_{\mathrm{v}}}{\mu_{\mathrm{l}}}\right)^{0.19}\left(1-\frac{\mu_{\mathrm{v}}}{\mu_{\mathrm{l}}}\right)^{0.7}$$
$$Fr = \frac{G^2}{gD\rho_{\mathrm{TP}}^2}, \quad We = \frac{G^2D}{\rho_{\mathrm{TP}}\sigma}, \tag{16}$$

where f_{v} and f_{l} are the friction factors for the total mass flux flowing with vapour and liquid properties, respectively, and ρ_{TP} is the homogeneous model density

$$\rho_{\mathrm{TP}} = \left(\frac{x}{\rho_{\mathrm{v}}} + \frac{1-x}{\rho_{\mathrm{l}}}\right)^{-1}.$$

In the accelerational term,

$$G^2\frac{\mathrm{d}}{\mathrm{d}z}\left(\frac{x^2}{\alpha\rho_{\mathrm{v}}} + \frac{(1-x)^2}{(1-\alpha)\rho_{\mathrm{l}}}\right),$$

and in the static head pressure term, $g(\alpha\rho_{\mathrm{v}} + (1-\alpha)\rho_{\mathrm{l}})$, the void fraction α is calculated with using the classical equation:

$$\alpha = 1\Big/\left\{1 + s\left(\frac{1-x}{x}\right)\left(\frac{\rho_{\mathrm{v}}}{\rho_{\mathrm{l}}}\right)\right\}, \tag{17}$$

where the slip ratio s is given by the correlation of Premoli et al. [13].

2.4. Liquid film flow rate

In diabatic annular flow, some complex mass transfer phenomena occur at the liquid–vapour interface of the liquid film. As is shown in Fig. 2, liquid droplets are continuously entrained from the liquid film into the vapour core, while, at the same time, some liquid droplets are deposited on the liquid surface. Besides, the vapour core is supplied with the liquid evaporated at the liquid–vapour interface and with the vapour bubbles due to the boiling process in the liquid film. Based on these observations, the liquid film flow rate can be calculated, as a function of the distance z along the channel, with the following equation (see also [14]):

$$\frac{\mathrm{d}W_{\mathrm{lf}}}{\mathrm{d}Z} = \pi D\left(d - e - \frac{q''}{\lambda}\right), \tag{18}$$

where w_{lf} is the liquid film mass flow rate, d is the liquid droplets deposition rate per unit area, e is the liquid droplets entrainment rate per unit area, q'' is the heat flux and λ is the latent heat of evaporation.

The droplets deposition rate, d, is calculated with the equation given by Kataoka and Ishii [15]:

$$\frac{dD}{\mu_{\mathrm{l}}} = 0.22Re_{\mathrm{l}}^{0.74}\left(\frac{\mu_{\mathrm{v}}}{\mu_{\mathrm{l}}}\right)^{0.26}E^{0.74}, \tag{19}$$

where μ_{l} and μ_{v} are the liquid and vapour viscosity, respectively, Re_{l} is the liquid Reynolds number, and E is the fraction of liquid flowing as droplets in the vapour core.

The droplet entrainment rate, e, is calculated considering the contribution of two different mechanisms of droplets formation: breakup of disturbance waves and boiling in the liquid film. According to Kataoka and Ishii [15], droplet entrainment is mainly attributed to the breakup of large disturbance waves on the liquid–vapour interface. Regarding the second mechanism of droplet formation, according to Mishima et al. [4], burst of boiling bubbles in the liquid film may cause droplet entrainment at sufficiently high heat fluxes. Since CHF reaches relatively high values, especially for small L/D ratios, considerable amount of liquid may be entrained in the vapour core by this process. Therefore, droplet entrainment rate e, is the sum of two quantities, such as e_{w} (entrainment due to disturbance waves) and e_{B} (entrainment due to boiling in the liquid film): $e = e_{\mathrm{w}} + e_{\mathrm{B}}$.

The wave entrainment rate e_{w} is evaluated by with the following equations [15]:

$$\text{if } E/E_\infty \leqslant 1,\ \frac{e_{\mathrm{w}}D}{\mu_{\mathrm{l}}} = 0.72\times10^{-9}Re_{\mathrm{l}}^{1.75}We(1-E_\infty)^{0.25}\times(1-E/E_\infty)^2 \tag{20}$$

$$\text{if } E/E_\infty > 1,\ \frac{e_{\mathrm{w}}D}{\mu_{\mathrm{l}}} = 0.22Re_{\mathrm{l}}^{0.74}\left(\frac{\mu_{\mathrm{v}}}{\mu_{\mathrm{l}}}\right)E_\infty^{0.74} \tag{21}$$

$$\text{if } Re_{\mathrm{lf}} < Re_{\mathrm{lfc}}\, e_{\mathrm{w}} = 0, \tag{22}$$

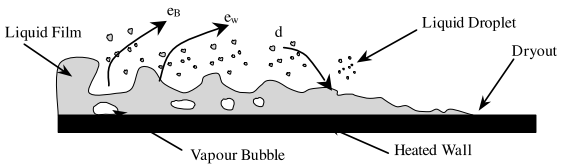

Fig. 2. Liquid film and dryout location.

where $E = (j_l - j_{lf})/j_l$ is the fraction of liquid entrained in the vapour core, E_∞ is the equilibrium entrainment fraction [16], $E_\infty = \tanh(7.25 \times 10^{-7}\eta)$, η is a non-dimensional parameter $\eta = We^{1.25}Re_l^{0.25}$, We is the Weber number for entrainment,

$$We = \frac{\rho_v j_v^2 D}{\sigma}\left(\frac{\Delta\rho}{\rho_v}\right)^{1/3},$$

Re_l is the liquid Reynolds number,

$$Re_l = \frac{G(1-x)D}{\mu_l},$$

and Re_{lf} is the liquid film Reynolds number:

$$Re_{lf} = \frac{G(1-x)(1-E)D}{\mu_l}. \tag{23}$$

The minimum liquid film Reynolds number, Re_{lfc}, below which no droplet entrainment due to superficial waves occurs [17], is given by:

$$Re_{lfc} = \left(\frac{y^+}{0.347}\right)^{1.5}\left(\frac{\rho_l}{\rho_v}\right)^{0.75}\left(\frac{\mu_v}{\mu_l}\right)^{1.5}, \tag{24}$$

where y^+ is the non-dimensional distance associated with the onset of the entrainment. For the present model, y^+ is equal to 10.

The boiling entrainment rate e_B can be calculated from the correlation of Ueda et al. [18], who studied falling liquid films on heated vertical tubes:

$$\frac{e_B\lambda}{q''} = 4.77 \times 10^2\left(\frac{q''2\delta}{\lambda^2\sigma\rho_v}\right)^{0.75}. \tag{25}$$

The liquid film thickness, δ, is calculated using the von Karman [19] universal velocity profile and assuming no bubble present in the liquid film.

2.5. Liquid film thickness

The liquid film thickness δ is calculated through the evaluation of the mean liquid velocity in the liquid film. Assuming a first attempt value for the liquid film thickness δ, it is possible to calculate the mean liquid film velocity in two different ways: by integrating the von Karman universal velocity profile in the film thickness, and by the mass balance in the film flow where mass flow rate is evaluated with Eq. (18).

For the calculation of the liquid film mean velocity with the universal profile the following assumptions are made:

1. the liquid film thickness is small in comparison with D;
2. the shear stress is constant through the liquid film and equal to the wall shear stress;
3. the whole liquid phase flows in the liquid film on the heated wall. The von Karman velocity profile is given by the following well-known equations:

$$u^+ = y^+, \quad 0 \leqslant y^+ \leqslant 5, \tag{26}$$

$$u^+ = 5\ln(y^+) - 3.05, \quad 5 \leqslant y^+ \leqslant 30, \tag{27}$$

$$u^+ = 2.5\ln(y^+) + 5.5, \quad y^+ > 30, \tag{28}$$

where

$$\tau_w = \frac{f u_{lf}^2 \rho_l}{8}, \quad U_\tau = \left(\frac{\tau_w}{\rho_l}\right)^{0.5}, \quad u^+ = \frac{u}{U_\tau} \tag{29}$$

$$y^+ = \frac{yU_\tau\rho_l}{\mu_l}, \quad u_{lf} = G\left(\frac{1-x}{1-\alpha}\right)\frac{1}{\rho_l} \tag{30}$$

In the above equations, u^+ is the dimensionless liquid velocity, y^+ is the dimensionless distance from the wall, τ_w is the wall shear stress, and f is the friction factor calculated with the Blasius equation $f = 0.3164Re^{0.25}$, where $Re = (j_l D\rho_l)/\mu_l$, being j_l the liquid superficial velocity.

For a given value of the liquid film thickness δ, Eqs. (26)–(28) allow to calculate the mean liquid velocity in the liquid film, $u_{lf,m}$, with the integral

$$u_{lf,m}^+ = \frac{1}{\delta^+}\int_0^{\delta^+} u^+ \,\mathrm{d}y^+. \tag{31}$$

The value of δ^+ is given by y^+ equation with $y = \delta$.

On the other hand, with the same thickness value δ above introduced, it is possible to calculate the mean liquid velocity with the mass balance $u_{lf,m} = w_{lf}/A_{lf}\rho_l$, where w_{lf} is the film mass flow rate evaluated with Eq. (18) and $A_{lf} = (\pi/4)(D^2 - (D-2\delta)^2)$ is the area occupied by the liquid flowing in the film with δ as thickness. So, as already said, given a liquid film thickness value, the mean liquid film velocity can be calculated with two equations: one from the universal velocity profile and the other one from the mass balance in the liquid film with mass flow rate given by Eq. (18). According to an iterative procedure, when the two equations for the mean liquid film velocity evaluation give the same value, the corresponding δ is assumed to be the actual liquid film thickness.

2.6. Flow regime transitions in saturated flow boiling region

In the present model, the criterion of the flow regime transition to annular flow is that proposed by Mishima and Ishii [20]. The transition from churn to annular flow (Fig. 1) occurs with collapse of liquid slugs associated with the formation of large disturbance waves and the onset of droplet entrainment. Annular flow is assumed to start when

$$j_v \geqslant \left(\frac{\sigma g\Delta\rho}{\rho_v^2}\right)^{0.25} N_{\mu_l}^{-0.2} \tag{32}$$

Table 1
Summary of CHF experimental values

Name	No. of exp. pts.	p_{ex} (bar)	G (kg m^{-2} s)	T_{in} (°C)	D (mm)	Z/D	q''_{exp} (kW m^{-2})	x_{exp}
Becker [24]	1884	2–100	100–8200	−25–270	3.9–25	3–380	500–52,000	0.0–1.0
Beus [25]	130	27–160	425–4660	90–315	9.5	194	388–4073	0.0–0.9
Kureta [26]	972	1.0	10–19,000	6–100	1.0–6.0	1–113	35–160,000	0.0–1.0
Lowdermilk [27]	551	1.0	27–34,000	21–100	1.3–4.8	25–250	167–41,600	0.0–1.0
Griffel [28]	402	34–70	350–2700	130–270	6–23.6	70–150	1600–3000	1.0
Macbeth [29]	1553	1.0–110	10–18,000	0.0–295	1–37.3	8.5–365	100–21,000	−0.25–1
Waters [30]	1217	30–200	150–8000	4–315	10.0	100–300	250–5500	−0.8–1

where N_{μ_l} is the viscosity number defined as

$$N_{\mu_l} = \left(\frac{\rho_l \sigma}{\sqrt{\sigma / g \Delta\rho}} \right)^{-0.5},$$

where j_v is the superficial vapour velocity, σ the surface tension, g is the gravitational acceleration and $\Delta\rho$ is the density difference between the two phases. In a previous study of Whalley et al. [21], the value for the entrainment fraction starting point of annular flow is assumed to be in the range from 0.9 to 0.99. Some existing data on the variation of entrainment fraction along the stream, however, indicate that the initial entrainment fraction is rather small. Therefore, it is assumed here that the initial entrainment fraction is only given by the contribution from the boiling entrainment.

2.7. Dryout mechanism

According to Saito et al. [2], although the CHF occurs when the liquid film is too thin and breaks down into rivulets around dry patches, it is reasonable to assume as the CHF criterion the vanishing of the liquid film. Therefore, the CHF is reached when the liquid film flow rate is zero at the exit of the heated channel (Fig. 2).

3. Results

In order to validate the model, a wide data set of 6709 CHF experimental points has been collected (see Table 1). The model was tested only tested on those experimental points (5159) which verify the following conditions:

1. the flow regime is turbulent ($Re > 2500$);
2. the outlet exit quality is positive ($x_{ex} > 0$);
3. the flow pattern at the CHF is annular flow.

The annular flow regime is verified through the the flow regime of Hewitt and Roberts [22], Taitel and Dukler [23] and Mishima and Ishii [20]. The three transition methods are adopted in order to avoid an eventual low precision in flow pattern identification of a single method, especially near the boundary between churn and annular flow. For the flow regime identification the experimental CHF value is used in calculations.

In Figs. 3–10, the ratio between calculated and experimental CHF is plotted versus thermal hydraulic parameters (x_{exp}, x_{out}, G, p_{out}, Z_{ann}/Z) and geometric parameters ($Z/D, D$).

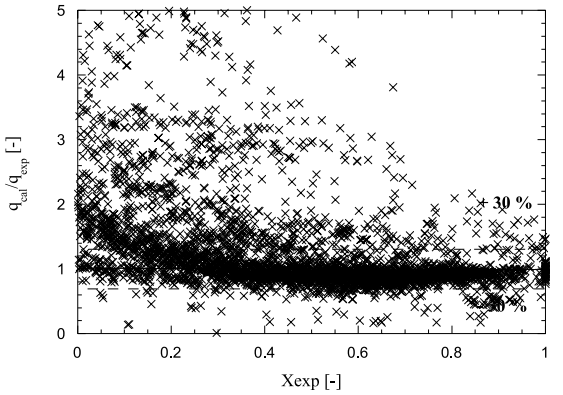

Fig. 3. Calculated to experimental CHF versus experimental exit quality x_{exp}.

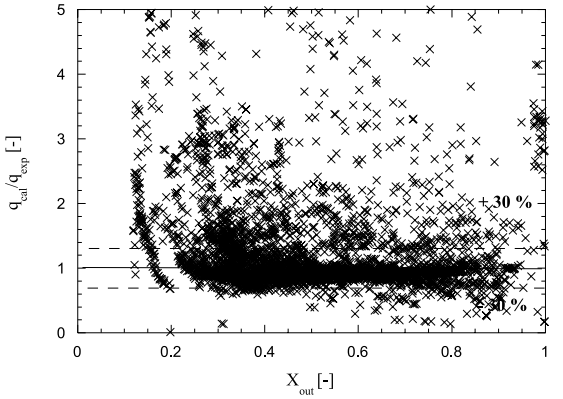

Fig. 4. Calculated to experimental CHF versus calculated exit quality x_{out}.

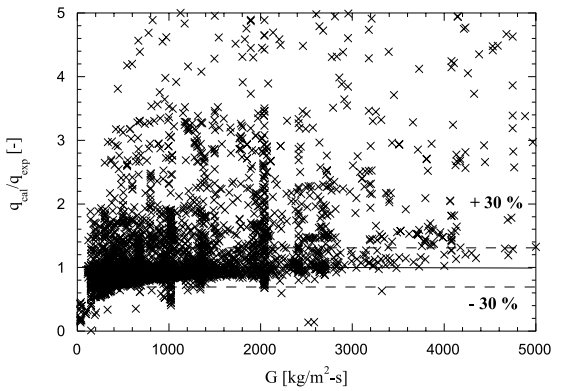

Fig. 5. Calculated to experimental CHF versus mass flux G.

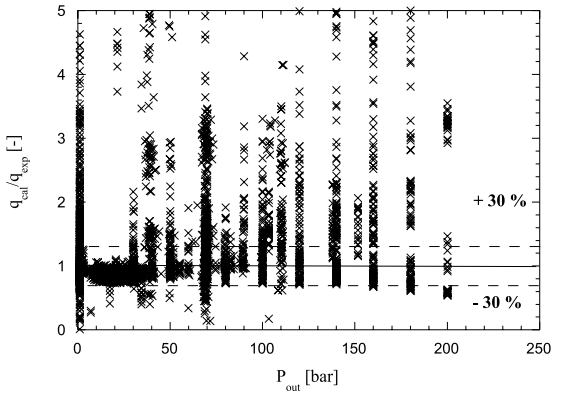

Fig. 6. Calculated to experimental CHF versus exit pressure p_{ex}.

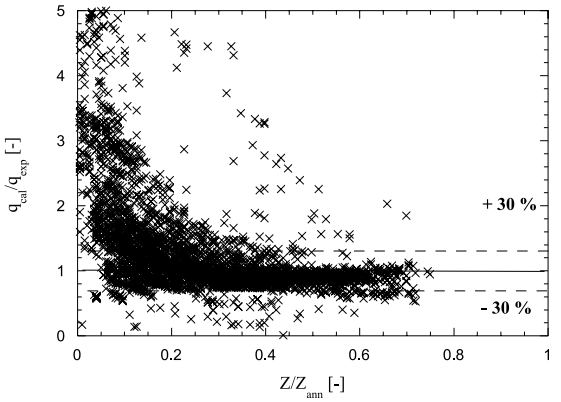

Fig. 7. Calculated to experimental CHF versus heated channel length fraction where annular flow boiling occurs.

In Figs. 3 and 4 a sensible systematic effect of the experimental and calculated liquid quality can be observed. In fact, in the case of the perfect model

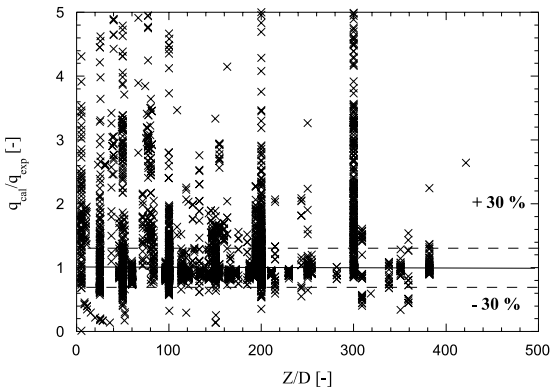

Fig. 8. Calculated to experimental CHF versus Z/D ratio.

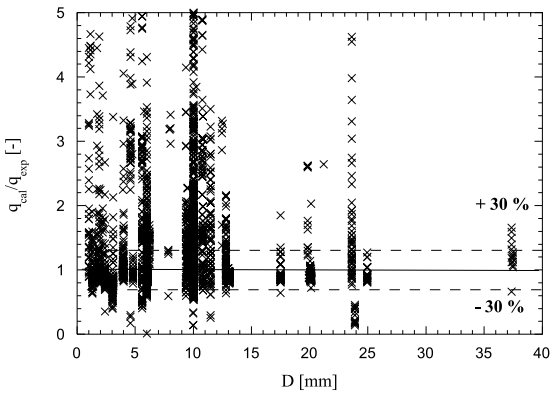

Fig. 9. Calculated to experimental CHF versus internal tube diameter D.

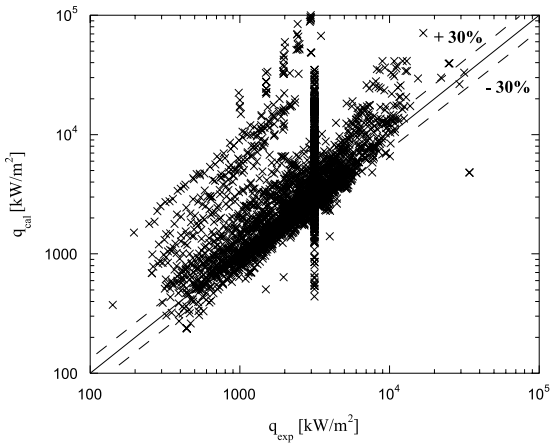

Fig. 10. Calculated versus experimental CHF on the whole data set.

prediction capability, these two graphs should have the same trend. But, actually in the low quality region there is a discrepancy between experimental and calculated exit quality. In particular, the model shows the tendency to overpredict the CHF calculation in the low quality region ($x_{out} < 0.2$). In this region, even if the flow regime is annular, the thermal crisis mechanism is likely DNB type and the model assumption about the Dryout mechanism looses its validity. On the other hand, as the boundary between DNB and Dryout CHF type regions is not clearly defined, it can be reasonably placed in the lower quality region. Therefore the model worst performance is concentrated in this region. Later in the discussion, the model tendency to overpredict the CHF in the low quality region will be explained.

Mass flux (Fig. 5) seems to have a slight significant influence on the model prediction capability for low values. Exit pressure (Fig. 6) seems not to have an influence on the CHF prediction. Fig. 7 shows the relation between the CHF calculation and the heated channel length fraction, Z_{ann}/Z, where the annual flow occurs. Most of overpredicted points are placed in the region of small annular flow length ($Z_{ann}/Z < 30$–35%). When annular flow regime occurs in a small portion of the heated channel, the reference conditions adopted in the model are no longer valid. In particular the liquid film dryout mechanism is not completely appropriate in order to describe the physical phenomena at CHF. In this situation the liquid film thickness becomes thick and the thermal crisis is probably influenced by the formation of vapour bubbles in the liquid film. When the liquid film thickness becomes thick, the present model gives exaggerate CHF values, with calculated critical heat flux values up to 30–40 times the experimental ones. In fact, from mathematical point of view, the model increases the predicted CHF in order to get smaller liquid film thickness and the dryout at the channel exit. This situation typically occurs in the low quality region as shown in Fig. 3.

Geometric parameters (Z/D and D) do not show any systematic influence on the CHF prediction (Figs. 8 and 9).

Fig. 10 shows the global comparison of calculated versus experimental CHF for all experimental points of the data set. About 65% of all calculated data points are within the error range $\pm 30\%$ and the R.M.S. is about 270%. In order to give an assessment of the actual model potential, it is convenient to consider the effect of the annular flow length as above explained. The model shows a quite good CHF prediction capability for Z_{ann}/Z larger than >35%, with about 92% of data points within the error range $\pm 30\%$ and a R.M.S. of 28%. Therefore, it is reasonable to consider the model applicable for annular flow length higher than 30–35 % of the channel length.

4. Conclusions

A new model for the evaluation of the CHF in under saturated flow boiling conditions is proposed. The flow regime at the CHF occurrence is assumed to be annular flow. The condition that triggers the CHF is when the liquid film vanishes at the heated channel outlet (dryout). The model is tested over a data set of 5159 selected experimental points. The model shows a quite good CHF predictive capability for those experimental points where annular flow occurs in a portion larger than 35% of the channel length ($Z_{ann}/Z > 35\%$), with about 92% of data points within the error range $\pm 30\%$ and a R.M.S. of 28%. Generally this situation occurs in region characterised by vapour quality higher than 0.2–0.3.

In those cases where annular flow occurs in a short length, especially in low quality region, the thermal crisis mechanism is DNB type and is different from that (dryout) postulated in the model. In such cases the model assumptions are not longer valid and the prediction capability is poor.

Acknowledgements

Part of the present work has been carried out with the support of the Fellowship Program of the Matsumae International Foundation in the period from 1 May to 26 September 1995.

References

[1] P.B. Whalley, The calculation of dryout in rod bundles, Int. J. Multiphase Flow 3 (1977) 501–515.
[2] T. Saito, E.D. Hughes, M.W. Carbon, Multi-fluid modelling of annular two-phase flow, Nucl. Eng. Des. 50 (1978) 225–271.
[3] S. Sugawara, Analytical prediction of CHF by FIDAS code based on three-fluid and film-dryout model, J. Nucl. Sci. Technol. 27 (1) (1990) 12–29.
[4] K. Mishima, H. Nishihara, K. Yamamoto, Dryout model for critical heat flux at high and intermediate quality region, Reprint from Annual reports of the Research Reactor Institute, Kyoto University 22 (1989) 1–13.
[5] F.W. Dittus, L.M.K. Boelter, Heat transfer in automobile radiators of the tubular type, University of California at Berkeley, Publication in Engineering 2 (13) (1930) 443–461.
[6] A.E. Bergles, W.M. Rohsenow, The determination of forced-convection surface boiling heat transfer, J. Heat Transfer 86 (1964) 365–372.
[7] W.M. Kays, M.E. Crawford, Convective Heat and Mass Transfer, second ed., McGraw-Hill, New York, 1980, p. 280 (Chapter 14).
[8] H. Schlichting, Boundary Layer Theory, sixth ed., McGraw-Hill, New York, 1968.

[9] S. Levy, Forced convection subcooled boiling – prediction of vapour volumetric fraction, Int. J. Heat Mass Transfer 10 (1967) 951–965.
[10] F.W. Staub, The void fraction in subcooled boiling – prediction of the initial point of net vapour generation, J. Heat Transfer 90 (1968) 151–159.
[11] L. Friedel, New friction pressure drop correlations for upward, horizontal and downward two-phase pipe flow, in: Proceedings of HTFS Symposium, Oxford, 1979.
[12] A.M. Lezzi, A. Niro, Cadute di pressione per acqua in ebollizione forzata in tubi di piccolo diametro, in: Proceedings of the 13th UIT Heat Transfer Conference, Bologna, Italy, 1995 (in Italian).
[13] A. Premoli, D. Francesco, A. Prina, A dimensionless correlation for determining the density of two-phase mixtures, La Termotecnica 25 (1971) 17–25.
[14] A.E. Bergles, J.G. Collier, J.M. Delhaye, G.F. Hewitt, F. Mayinger, Two-Phase Flow and Heat Transfer in the Power and Process Industries, first ed., Hemisphere, New York, 1981, pp. 274–278.
[15] I. Kataoka, M. Ishii, Entrainment and deposition rates of droplets in annular two-phase flow, in: Y. Mori, W.J. Yang (Eds.), Proceedings of the ASME/JSME Thermal Engineering Joint Conference, vol. 1, 1983.
[16] M. Ishii, K. Mishima, Droplet entrainment correlation in annular two-phase flow, Int. J. Heat Mass Transfer 32 (10) (1984) 1835–1846.
[17] M. Ishii, M.A. Grolmes, Inception criteria for droplet entrainment in two-phase concurrent film flow, AIChE J. 21 (1975) 308–319.
[18] T. Ueda, M. Inoue, S. Nagatome, Critical heat flux and droplet entrainment rate in boiling of falling liquid films, Int. J. Heat Mass Transfer 24 (7) (1981) 1257–1266.
[19] T. von Karman, Analogy between fluid friction and heat transfer, Trans. ASME, Series C 61 (1939) 705–719.
[20] K. Mishima, M. Ishii, Flow regime transition criteria for upward two-phase flow in vertical tubes, Int. J. Heat Mass Transfer 27 (5) (1984) 723–737.
[21] P.B. Whalley, P. Hutchinson, G.F. Hewitt, The calculation of critical heat flux in forced convection boiling, in: Proceedings of the Fifth International Heat Transfer Conference, Tokyo, Paper B6, 1974, pp. 290–294.
[22] G.F. Hewitt, D.N. Roberts, Studies of two-phase flow patterns by simultaneous X-ray and flash photography, AERE-M 2159, HMSO, 1969.
[23] Y. Taitel, A.E. Dukler, Modelling flow pattern transition for steady upward gas liquid flow in vertical tubes, AIChE J. 26 (3) (1980) 345–352.
[24] K.M. Becker, Burnout data of boiling water in vertical round ducts, annuli and rod clusters, Aktiebolaget Atomenergi Report AE177, Sweden, 1965.
[25] C.L. Williams, S.G. Beus, Critical heat flux experiments in a circular tube with heavy water and light water (AWBA Development Program), WAPD-TM-1462, Westinghouse Electric Corporation, Pittsburg, PA, 1980.
[26] M. Kureta, K. Mishima, H. Nishihara, Critical heat flux for flow-boiling of water in small-diameter tubes under low-pressure conditions, Trans. Jpn. Soc. Mech. Eng., Series B 61 (595) (1996) 4109–4116 (in Japanese).
[27] W.H. Lowdermilk, C.D. Lanzo, B.L. Siegel, Investigation of boiling burnout and flow stability for water flowing in tubes, Technical note 4382, NACA Washington, 1958.
[28] J. Griffel, Forced convection boiling burnout for water in uniformly heated tubular test sections, USAEC Report NYO 187-7, TID-4500, 1965.
[29] R.V. Macbeth, B. Thomson, Boiling water heat transfer. Burnout in uniformely heated round tubes: a compilation of world data with accurate correlations, Technical note 4382, NACA Washington, 1958.
[30] E.D. Waters, Experimental observations of upstream boiling burnout, HW73902 (Rev), Handford Atomic Products Operation, Richland WA, November, 1962.